energies

MDPI

Article

Theoretical Analysis of the Effect of Electrical Heat In Situ Injection on the Kerogen Decomposition for the Development of Shale Oil Deposits

Maryelin Josefina Briceño Montilla [1,2,3], Shouding Li [1,2,3,*], Zhaobin Zhang [1,2,3,*], Xiao Li [1,2,3], Yiming Sun [1,2,3] and Shiwei Ma [1,2,3]

[1] Key Laboratory of Shale Gas and Geoengineering, Institute of Geology and Geophysics, Chinese Academy of Sciences, Beijing 100029, China
[2] Institute of Earth Sciences, Chinese Academy of Sciences, Beijing 100049, China
[3] College of Earth and Planetary Sciences, University of Chinese Academy of Sciences, Beijing 100049, China
* Correspondence: lsdlyh@mail.iggcas.ac.cn (S.L.); zhangzhaobin@mail.iggcas.ac.cn (Z.Z.)

Abstract: In situ heat injection is a suitable technique for extracting shale oil from reservoirs with high organic matter content but insufficient thermal maturation. To optimize the stimulation process and to avoid unnecessary energy consumption, understanding the thermal process and the effects of thermal parameters is crucial. This research employs a self-developed simulator to build a 2D numerical model of the in situ conversion process of kerogen with electric heaters. A benchmark model is first established to determine the effects of heat injection on crude oil production and kerogen decomposition. Subsequently, this study analyzes the evolution of shale oil within the reservoir, identifying the role of thermal and physical properties in crude oil production and kerogen decomposition during the stimulation treatment. A sensitivity analysis of the thermal properties of the reservoir is also carried out, which allows for defining the role of the thermal conductivity of the rock during the stimulation process. Finally, it is observed that, when using the injection at a constant power, the injection time to achieve a suitable large rate of decomposition is shorter than at a constant temperature—consequently, it has a higher economic advantage.

Keywords: in situ conversion; kerogen decomposition; numerical model; heat transfer

check for updates

Citation: Briceño Montilla, M.J.; Li, S.; Zhang, Z.; Li, X.; Sun, Y.; Ma, S. Theoretical Analysis of the Effect of Electrical Heat In Situ Injection on the Kerogen Decomposition for the Development of Shale Oil Deposits. *Energies* **2023**, *16*, 5007. https://doi.org/10.3390/en16135007

Academic Editor: Riyaz Kharrat

Received: 20 April 2023
Revised: 21 June 2023
Accepted: 23 June 2023
Published: 28 June 2023

Copyright: © 2023 by the authors. Licensee MDPI, Basel, Switzerland. This article is an open access article distributed under the terms and conditions of the Creative Commons Attribution (CC BY) license (https://creativecommons.org/licenses/by/4.0/).

1. Introduction

Shale oil is a liquid hydrocarbon extracted from organic-rich shale and/or mudstone rock formations that have not reached enough of a thermal maturity to generate hydrocarbons [1,2]. A comprehensive study conducted by the U.S. Energy Information Administration and Advanced Resources International, Inc. in 2013 estimated a total of 1073 million cubic meters of technically recoverable shale oil resources worldwide. Notably, Russia, the United States, China, and Argentina ranked as the top four countries with significant technically recoverable shale oil reserves [3]. The in situ conversion process has emerged as a viable technology for economically extracting these resources [4,5]. As in situ conversion is still a relatively new and experimental technology, there are considerable challenges to address. Nevertheless, it shows promise as a potential source of domestic energy and provides an opportunity to extract oil from shale formations that would otherwise be inaccessible using traditional drilling methods. This complex technique involves fluid flow, heat transfer, and the chemical decomposition of organic matter [6,7]. Given the heterogeneity of oil shale reservoirs, it becomes crucial to comprehend heat injection behavior in this type of formation. Therefore, simulation models play an essential role in predicting and studying the diverse mechanisms involved.

In recent years, considerable attention has been given to the development of simulation models for in situ conversion, particularly in simulating pyrolysis processes at the reservoir level and understanding the correlation between temperature increases and kerogen

decomposition. Fan et al. [8] used their self-developed simulator to model the Shell in situ conversion process (ICP) in the Green River data, using 16 heaters at constant temperature injection. Their studies focused on the sensitivity analysis of the heater pattern injection and position. Hazra [9] conducted an analysis of different heating schemes and configurations using CMG STARTS commercial software, performing a sensitivity analysis to compare the energy efficiency of various in situ retorting technologies. Egboga et al. [10] investigated thermal stimulation techniques for enhancing oil recovery in the early-stage depletion of the Bakken formation. Lee et al. [11] extended the TAMU Flow and Transport Simulator (FTSim) to incorporate kerogen pyrolysis in the Green River Formation base in the Shell ICP project data. Their analysis examined the effects of porosity, oil shale grades, and fracture spacing on hydrocarbon production. Huang et al. [12] developed a comprehensive coupled thermo-hydro-mechanical-chemical model to investigate the mechanism and influence of engineering parameters in in situ conversion. Shi et al. [13] studied the relationship between energy utilization efficiency and oil output under different operational conditions. The primary objectives of these investigations have been to simulate the chain reactions involved in the in situ decomposition process, to analyze the productivity of the different thermal stimulation methods, and to study the injection conditions of each method.

In the thermal methods of oil recovery, the efficient delivery of heat to the reservoir from the heat source strongly depends on the heat transfer through the reservoir media [14]. However, despite the success of thermal recovery in conventional reservoirs, the relationship between heat flow and geological formations remains unclear. The analysis of the thermal characteristics is more complex in shales with organic matter content [15]. Factors such as porosity, permeability, and lithology significantly influence the thermal conductivity, heat capacity, and thermal diffusion coefficient of rocks [16,17]. Moreover, the heat transfer characteristics of oil shale rocks show anisotropy due to their sedimentary properties and natural fractures [18]. Consequently, any changes in thermal properties directly influence temperature distribution and the efficiency of thermal methods. Therefore, it is important to understand the thermal process and the effects of the thermal parameters in in situ heating. This understanding provides insights into the energy requirements for obtaining an efficient stimulation process, thereby helping to avoid unnecessary energy consumption.

In this research, the effects of thermal parameters on kerogen decomposition during the in situ conversion process are examined via a self-developed simulator. Initially, a benchmark model is built to study the effects of decomposition on the production of liquid hydrocarbon. The analysis focuses on temperature evolution and identifies the effects of rock conductivity on the decomposition process. Subsequently, a sensitivity analysis is conducted to determine how the thermal properties of the rock affect kerogen decomposition. Additionally, the importance of heat sources in proximity to producing wells is discussed. Finally, a comparison is made between injection at constant temperature and injection at constant power to assess the efficiency of both methods on oil production.

The self-developed simulator used in this study was programmed in Python and is an extension of the hydrate methane software used by [19]. The numerical simulation conducted consists of a thermal–flow–chemical (TFC) model, which involves a non-isothermal temperature model to describe the heat transfer by conduction, as well as local thermal non-equilibrium to define the heat transfer by convection. The chemical model relies on the elementary rate law for a first-order reaction. The conductive heat transfer between the heaters and reservoir is calculated using the integrated conductive heat equation, while fluid drainage is described by the hydraulic conductivity equation. The verification model provides compelling evidence of the simulator's capability to model the physical and chemical phenomena associated with in situ conversion, making it a reliable tool for further investigations.

2. Numerical Model Method

For in situ kerogen decomposition, a self-developed numerical simulator is proposed, which considers mass transport, heat flow in porous media, and chemical decomposition.

The model is an extension of the hydrate methane software provided by [19]. In this research, the model includes four components (gas, oil, water, and kerogen), and four phases (aqueous, oily, gaseous, and solid), where the viscosity of the solid phase is set high to limit mobility. The chemical and multiphase component model has been verified through mathematical and laboratory experiments [20]. The research is focused on modeling the heat transfer in an in situ conversion treatment to study the effects of the thermal stimulation process and the thermodynamic transition of the hydrocarbon generated. Therefore, to make the simulation more stable in this research, several assumptions are considered: (1) The flow is linear and obeys Darcy's law. (2) The elemental rate law for a first-order reaction is assumed. (3) Only hydrocarbon liquids are computed. (4) The reaction heat is considered in the heat accumulation. (5) The fluid present is considered compressible. (6) The rock conductivity properties do not change during the simulation process.

2.1. Multiphase Flow Model

The mass and energy balance equation is expressed for each component i based on the following [21]:

$$\frac{d}{dt}\int_{V_n} M^i dV = \int_{\Gamma_n} \mathbf{F}^i \cdot n d\Gamma + \frac{d}{dt}\int_{V_n} q^i dV \tag{1}$$

where V_n in the volume of element n, Γ_n is the surface area of element n, M^i is the mass accumulation term for each component i, $\mathbf{F}^i$ is the flux vector, and q^i is the source/sink terms. The mass accumulation and flux term are computed by the following:

$$M^i = \sum_{j=G,A,O,S} \phi S_j \rho_j X_j^i \; i = g, w, o, k \tag{2}$$

$$\mathbf{F}^i = \sum_j F_j^i = \sum_j -K\frac{K_{r,j}\rho_j}{\mu_j}\left(\nabla P_j - \rho_j g\right) \tag{3}$$

where ϕ in the matrix porosity; S_j and ρ_j are the saturation and the density of phase j, respectively; and X_j^i is the mass fraction of the component $i = g, w, o, k$ (denoting gas, water, oil, and kerogen, respectively) in phase $j = G, A, O, S$ (denoting gaseous, aqueous, oily, and solid, respectively). F_j^i represents the multi-phase flow term that obeys Darcy's law. K and $K_{r,j}$ are the effective permeability and the relative permeability of the phase j, respectively; μ_j is phase viscosity; P_j is phase pressure; and g is the gravitational constant $\left(g = 10.0\ \mathrm{m/s^2}\right)$. The relative permeability is adopted using the modified version of Stone's method. This method assumes the effective permeability at S_{wirr} is $k_{row} = k_{rog} = 1$ at $S_g = 0$; $S_w = S_{wc}$; and the ends must satisfy $k_{row} = k_{rog}$ at $S_g = 0$.

$$k_{r,j} = \left(\frac{s_j - s_{ir,j}}{1 - S_{ir,j}}\right)^{n_j} \tag{4}$$

where s_j is the phase saturation, and $s_{ir,j}$ is the residual saturation. To account for multiple phases in the simulation, the reduction exponent has been set $n_j = 2$ to ensure the fluid resistance decreases rapidly. Additionally, S_{wirr} is set to zero to guarantee that the fluid can always flow. Those assumptions are settled to warrant computational stability.

The energy accumulation and heat flux term are given by the following:

$$M^\theta = (1 - \varnothing)\rho_R C_R T + \sum_{j=G,A,O,S} \varnothing S_j \rho_j U_j + Q_{diss} \tag{5}$$

$$Q_{diss} = \Delta\left(\varnothing \rho_k S_k \Delta H^0\right) \tag{6}$$

$$\mathbf{F}^{\theta} = -\bar{k}_{\theta}\nabla \mathrm{T} + \sum_{j} h_j F_j \tag{7}$$

where ρ_R is the matrix shale density, C_R is the heat capacity of the shale rock, U_j is the specific internal energy of the phase j, T is the temperature, Q_{diss} denotes the heat of the decomposition reaction, ρ_k is the density of kerogen, S_k is the kerogen saturation, and ΔH^0 is the specific enthalpy of decomposition. $\mathbf{F}^{\theta}$ is the heat flux term, $\bar{k}_{\theta}$ is the composite thermal conductivity of the shale rock, and h_j is the specific enthalpy of phase j.

2.2. Kerogen Decomposition

In the in situ conversion, the changes in the characteristics of the kerogen with temperature are commonly defined using a first-order kinetic reaction [8,10,11,22]. It is assumed that the reactions follow the elementary rate law, which allows for the determination of product quantities. Therefore, the reaction rate is computed as follows:

$$r_k = K_k C_k \tag{8}$$

where r_k is the reaction rate, K_k is the reaction rate constant, and C_k is the concentration of the reactant. The reaction constant is computed as stated in the Arrhenius equation:

$$K_k = A_k exp^{(-\frac{E_K}{RT})} \tag{9}$$

$$C_k = \varnothing S_j \rho_j X_j^i \tag{10}$$

where A_k and E_k are the frequency factor and activation energy of each reaction, respectively; R is the gas constant; and T is the temperature of the reaction.

In the chemical reaction, the quantities of reactants and products (expressed in terms of mass) are determined using Equations (11) and (12). These terms are then subtracted or added to the mass accumulation equation (Equation (2)), respectively.

$$M_{rea}^i = r_k \Delta t \tag{11}$$

$$M_{pro}^i = s_k r_k \Delta t \tag{12}$$

where Δt is the time step through which the reaction occurs, and the s_k is the ratio of a unit mass of products obtained per each unit mass of reactant.

2.3. Heat Injection

The boundary conditions indicate the initial heat distribution and the initial stimulation. Therefore, the source of heat is determined by the downhole injection method. For this research, the downhole heaters were set to a constant temperature. To regulate the downhole temperature, the cells containing heaters are assigned high values of heat capacity. The heat transfer by conduction is determined using thermal diffusivity, which describes the unsteady heat conduction k as a function of density ρ_R, and the specific heat capacity C_R of the shale rock is computed by the equation $a = k/\rho_R C_R$. The rate of heat transfer by conduction is calculated based on the length and area of the model's cell to distribute heat within the matrix. However, in order to simulate an ideal reservoir model, only conductive heat transfer in a radial direction from the injector well to the reservoir was considered. The conductive heat transfer was computed using the integrated conductive heat equation as follows:

$$\frac{Q}{dt} = \bar{k}_{\theta} A \frac{dT}{dr} = \frac{2\pi \bar{k}_{\theta} w}{\ln(R) - \ln(r_w)} \Delta T \tag{13}$$

where (Q/dt) is the heat conduction equation, $\bar{k}_\theta$ is the thermal conductivity of the shale matrix, r_w is the radius of the injection well, and w and R are the thickness and the radius of the altered zone by the heat, respectively. In this equation, it is assumed that the thermal conductivity is constant and isotropic.

2.4. Numerical Solving

Once the equations are discretized, and the initial and boundary conditions are given, the initial values of the unknown variables are assigned. The time step is calculated based on the previously calculated flow field, which is solved using the finite volume method. Subsequently, the flow fluid field (Equation (3)) and the fluid mass (Equation (2)) were combined with the mass conservation equation (Equation (1)) and transformed into a linear system, which is expressed in terms of pressure. This approach allows for the calculation of pressure values, flow rate, and fluid saturation values in the current time step. Using the updated saturation values, the convection process is naturally simulated by considering the sensible heat of fluids, which is dependent on the flow rate and fluid temperature (Equation (5)). Next, the heat conduction equation (Equation (6)) is solved using the finite volume method, and it is coupled with a linear system to determine the temperature of each cell. With the updated temperature values, the kerogen decomposition is computed, and the change in mass, temperature, and pressure are solved using a dichotomy method. The scheme of the numerical model is shown in Figure 1.

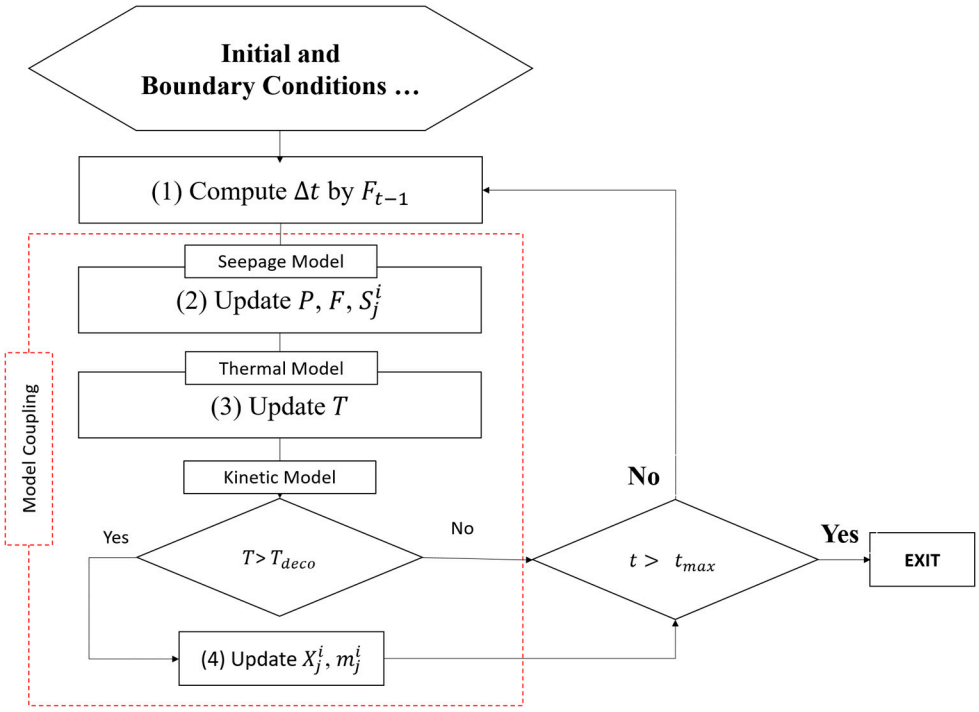

Figure 1. Scheme diagram of the calculation process.

2.5. Model Verification

The verification model used in this study is a coupled seepage, thermal, and chemical model that can predict the behavior of a reactant within a specific environmental context. In order to establish and calibrate the model, laboratory experiment data were used. The validity of the thermal model was assessed through an experiment that describes the evolution of temperature in a sedimentary rock under an exothermic reaction of $CaO + H_2O$. Similarly, the chemical model was verified by an experimental study focused on the thermal cracking reactions of ultra-heavy oils during assisted air injection. The key equations,

assumptions, and parameters involved in each model were carefully selected and adjusted to match the laboratory data.

To verify the heat transfer by conduction and convection within the thermal model, an experiment performed in the laboratory was used. Figure 2 presents the experimental setup employed in this study. The experiment consisted of an imitation wellbore, which is where the reaction occurs, and four monitoring points that define the location of the thermometers. The experiment setup is shown in Table 1.

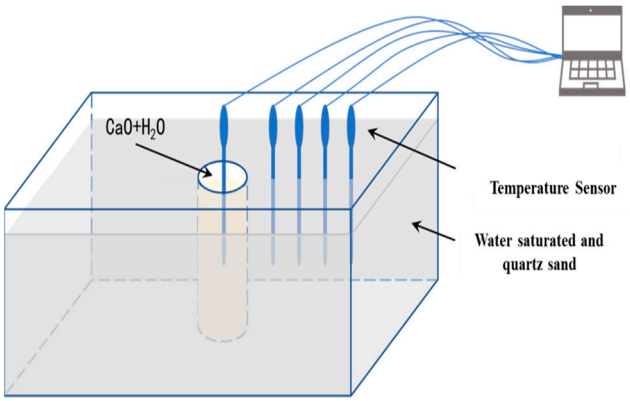

Figure 2. Scheme of the experiment.

Table 1. Experimental information.

Experimental Setup	
Sediments	Quartz sand (grain size: 120–180 mesh)
Porosity	0.38
Saturation	100% (distilled water)
Model Size	19.5 × 13 × 6 cm, imitation wellbore: 2.5 cm
Reactant	20 g CaO + 20 g water
Monitoring	1 thermometer in the wellbore, 4 in sediments with an interval of 1.6 cm. Depth: 3 cm
Initial temperature	24.5 °C

By controlling the energy release rate of the reaction, the simulator is capable of replicating the temperature elevation that occurs during the process of the reaction (Figure 3a). The obtained results show a noteworthy correspondence and conformity with the experiment data. The increased temperatures indicate that the duration of the reaction is 7 s approximately. Subsequently, the reaction stops, leading to a decline in temperature. In Figure 3b, the temperature variations across the monitoring points are presented, displaying a similar trend as was observed in the experiment. Nevertheless, the simulation reveals a more rapid decay in rock temperature compared to the experiment. This discrepancy arises from the absence of controls for the adjacent effects in the experiment. In addition, the simulation model is limited to a two-dimensional representation. Consequently, the simulation model fails to encompass the complete range of temperature conditions within the surrounding environment. Figure 4 illustrates the temporal and spatial evolution of temperature at the monitoring points, affirming the brief duration of thermal stimulation that was caused by the reaction. The close agreement observed in the simulations supports the notion that the logarithmic distribution pattern obeys the principles of the two-dimensional Fourier law.

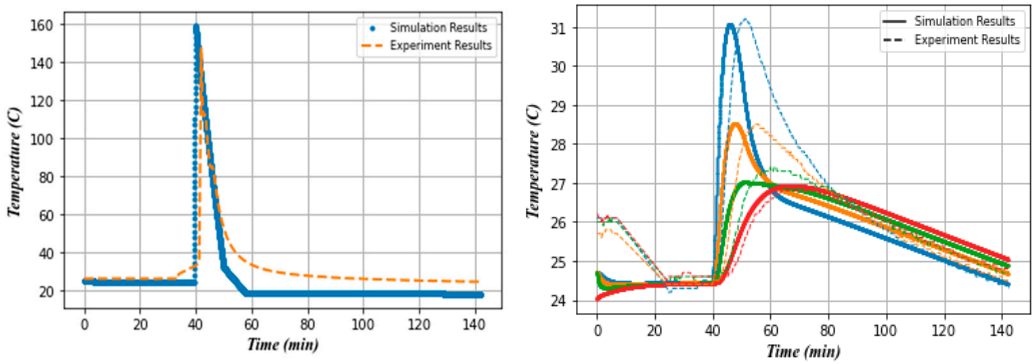

Figure 3. Results of the simulation: (**a**) in the injector well where the reaction is performed, and (**b**) temperature evolution in the monitoring points.

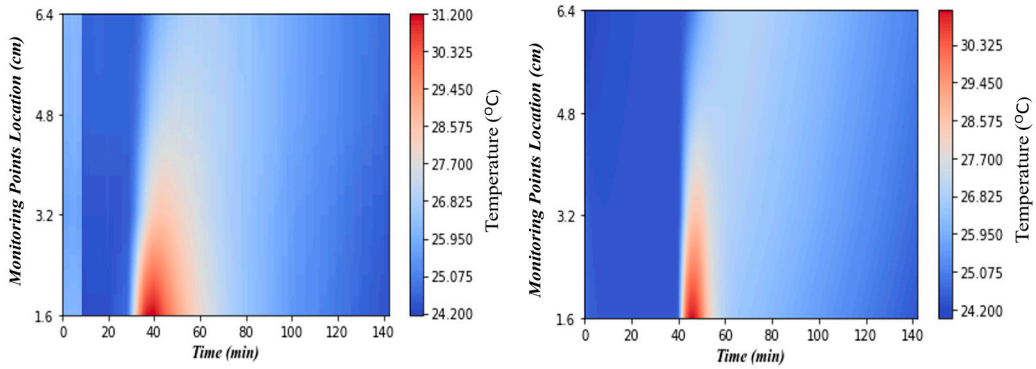

Figure 4. Evolution of the temperature field versus time. (**a**) Experiment results and (**b**) simulation results.

The robust agreement between the simulation results and the experimental data provides confidence in the reliability of the model. This substantiates the model's capability to accurately capture the dynamics of the temperature variations and validate the underlying principles governing the system.

To verify the chemical model, data from an experimental study on the thermal cracking of ultra-heavy oils during an air-injection-assisted method, as conducted by [23,24], were used. The basic properties of the ultra-heavy sample are presented in Table 2. The thermal cracking experiment was conducted under a temperature of 623.15 K and a pressure of 7.5 MPa. Kinetic reaction parameters, as shown in Table 3, were obtained based on the thermal cracking results. The selection and adjustment of these parameters for inclusion in the chemical model were performed to observe the chemical decomposition of the heavy oil that is based on elementary rate law. The simulation results exhibit a high degree of agreement with the experimental findings; this is because the chemical model accurately represents the mass fraction of each component at different time points, indicating a good degree of fitting (Figure 5).

Table 2. Properties of the heavy oil used in the experiment.

Oil Sample	Density (kg/m^3)	Viscosity (Pa·s)	Mass (kg)
Heavy Oil A *	1007	191.6	0.02

* Data provided by [23].

Table 3. Experimental results of the thermal cracking model calculation.

Reaction	Rate Constant K_k	Frequency Factor (1/s)	Activation Energy (J/mol)
	623.15 K		
HO → 0.5608LO + 0.1721Gas + 0.2671Coke *	8.45×10^{-7}	5.55×10^{14}	248,447

HO = heavy oil, Gas = mixed gas, and LO = light oil. * Data provided by [23].

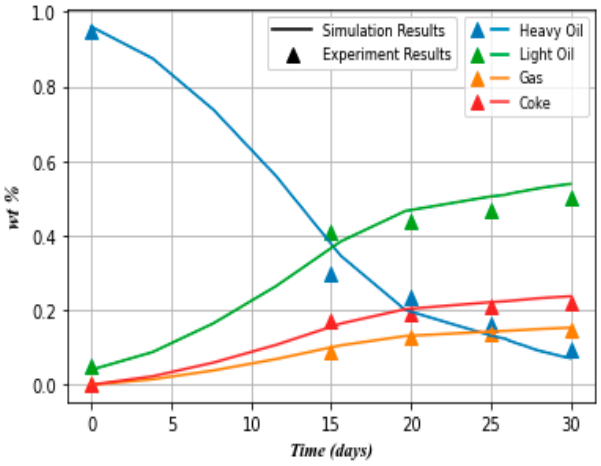

Figure 5. The simulation and experiment value results of oil components. Triangles represent the experiment data obtained after thermal cracking of the ultra-heavy oil in the presence of air.

The overall close agreement between the simulated and experimental results in terms of temperature, fluid, and chemical decomposition provides compelling evidence of the model's capability to accurately and efficiently analyze in situ conversion processes.

3. Results

3.1. Building Model

The simulation model is a 2D simulation of the in situ horizontal heat injection profile. Hence, the configuration of wells includes two horizontal injection wells that contain the heaters, along with a horizontal producing well in the middle (Figure 6a). The grid mesh consists of a 50 × 50 × 1.5 m grid of 2500 cells, resulting in a total volume of 7500 m^3. The heaters are located 5 m away from the producer well (Figure 6b). Research suggests that at temperatures above 500 K, kerogen undergoes decomposition, resulting in the formation of new hydrocarbons [23,25]. Therefore, the simulations are conducted by applying a constant injection temperature, starting at 900 K, to ensure that the kerogen decomposition temperature reaches a large number of the cells in the model. The simulated rock type consists of organic shale rock with ultra-low permeability, which contains shale oil, gas, and kerogen. The initial kerogen saturation is set at 60%, and the total mass content of kerogen is 2.9×10^6 kg.

Kerogen is a complex mixture of organic compounds, consisting of a high-molecular structure with a large organic carbon content [26,27]. Under thermal stimulation, kerogen decomposes into various bituminous products, which further crack into different low-carbon products [28]. Since this research focused on analyzing the expelled shale oil, we only calculated the decomposition of kerogen. Braun and Burnham simplified the kerogen decomposition process into eight compounds [29], which we have adopted for our model. Shale oil is defined as a mixture of light oil and heavy oil, while the gas is a combination of methane and other gases, and we adopted the presence of only one type of coke. Details of the chemical model are shown in Table 4. The thermal and transport properties of the fluids depend on pressure and temperature, and we assumed no chemical interactions between the oil components. The correlations used for these properties are listed in Table 5. We consider the released shale oil to consist of high-viscosity hydrocarbon. This is supported

by Onishchenko et al. [30], who show that kerogen destruction releases heavy hydrocarbon components. Therefore, the relationships for shale oil are based on the crude oil extracted from conventional reservoirs of heavy oil and bitumen [31,32]. The specific heat of the shale oil was computed according to the correlations from [33]. Additional reservoir data are displayed in Table 6.

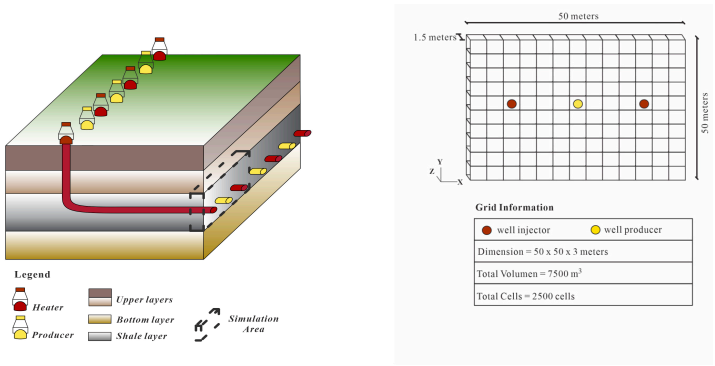

(**a**) (**b**)

Figure 6. (**a**) Scheme of the in situ heat injection process. (**b**) Scheme of the grid mesh model used in the simulation model.

Table 4. The chemical reaction equation modeled and the kinetic properties of the reaction.

Reaction [29]	**Rate Constant (1/s)**	**Activation Energy (Joules/Mol)**
	565 K	
Kerogen $\rightarrow$ 0.739Shale Oil + 0.046Gas + 0.215Coke	2.197×10^{-8}	161,600.0

Table 5. Correlations for the transport and thermal properties of the fluids.

Fluid	**Density**	**Viscosity**	**Specific Heat**
Shale Oil *	Nourozieh et al. [32]	Mehrotra and Svrcek [31]	1800 J/kg·K. [33]
Gas	EOS-Soave-Redlich Kwong. [34]	Yaw's Correlations. [35]	
Water	IAPW. [36]		

* Shale oil is considered as mixture of heavy oil and light oil.

Table 6. Input parameters in the numerical simulation.

Properties		**Units**	**Value**
Initial Conditions	Initial Temperature	K	338
	Initial Pressure	MPa	15.0
	Heating Temperature	K	900
	Bottom Hole Pressure	MPa	3.5
	Saturation	Sg	0.1
		Sw	0.0
		So	0.3
		Sk	0.6
Rock Properties	Permeability	m^2	1.0×10^{-15}
	Porosity	%	0.43
	Density [37]	kg/m^3	2600
	Heat Conductivity [18]	W/m·K	1.0
	Specific Heat [18]	J/kg·K	1000
Kerogen Properties [3]	Density	Kg/m^3	1200
	Specific Heat	J/kg·K	1500

3.2. Shale Oil Production Analysis

The objective of the in situ conversion method is to provide the potential development of shale with a high organic matter content. To assess the heat's effect on kerogen decomposition and oil production, the accumulated oil mass was measured in the producer well during the in situ treatment and compared with the accumulated production obtained through primary recovery.

Figure 7a reveals that, after 20 years of stimulation, oil production that uses the in situ method amounts to 127.78 $\times$ 10^3 kg, while the production by primary recovery is 1.03 $\times$ 10^3 kg. However, the results demonstrate that the effects of decomposition are not immediately observed in crude oil production. The accumulation of oil mass production increases slightly initially, then exhibits a remarkable increase after 7 years. This trend does not correlate with the initiation of kerogen decomposition. Figure 7b indicates that decomposition begins 70 days after the injection process has started. This delay can be attributed to the rock's low permeability and its limited heat conductivity, which will be explained later in detail.

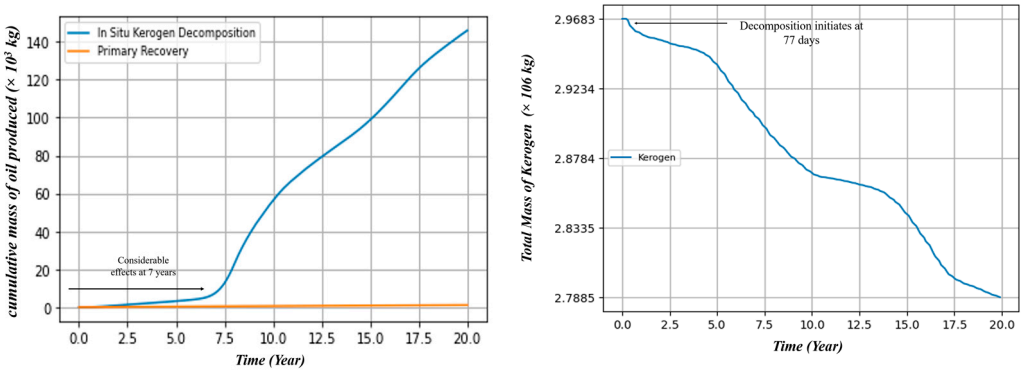

(**a**) (**b**)

Figure 7. (**a**) Comparison of the cumulative mass of oil under production between the in situ kerogen decomposition and the primary oil recovery. (**b**) Kerogen decomposition during the in situ treatment.

3.3. Kerogen Decomposition

As kerogen decomposition begins 72 days after injection, it indicates that the kerogen rapidly reaches the decomposition temperature. However, the temperature profile averaged in the transverse direction reveals that the maximum temperatures are reached around the injection wells, and that they tend to decrease as the injection points move away (Figure 8). Therefore, the initial quantities of oil expelled by decomposition are formed in the surrounding area of the injectors. The measurement of the temperature of the rock and the kerogen near the injector wells confirms that the kerogen starts its decomposition a few days after the treatment (Figure 9). It was observed that, during the first year of heating, there is a local thermal non-equilibrium response. This is because there is a minimal difference in the rate of temperature increase between the rock and the kerogen. Nonetheless, after 144 days of injection, the rock and the kerogen reach thermodynamic equilibrium.

3.4. Space–Time Evolution of Saturation and Temperature

In the production analysis, it is observed that the effect of the kerogen decomposition is not immediately reflected in the production. Instead, there is a transition stage where the production rate gradually increases during the first 6 years until it experiences a significant increase at 7.5 years. In this context, the evolution of the produced oil, the oil flowing through the porous spaces of rock, and the oil released by decomposition into the reservoir were analyzed. The three phases are described based on the oil production and the oil generated by decomposition (Figure 10).

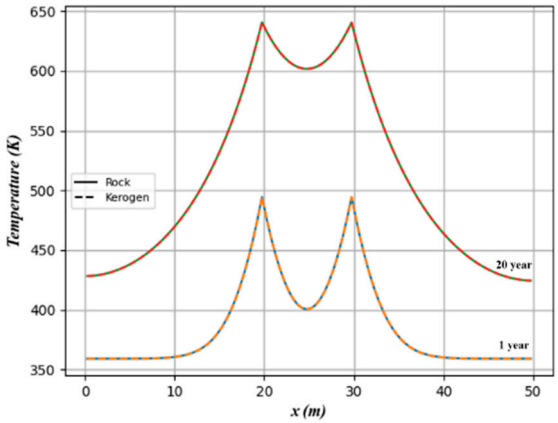

Figure 8. The temperature distribution profile averaged in the transversal direction around the area that was thermally stimulated from the minimal horizontal coordinate (x = 0 m) to the maximum horizontal coordinate (x = 50 m).

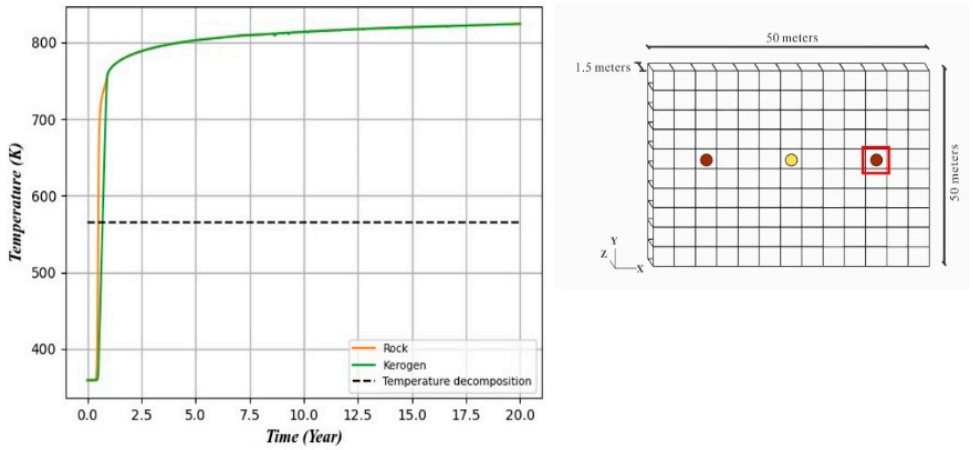

Figure 9. The temperature measurement nearby the injector well is indicated in the sub-figure. The rock and the fluid reach the thermal equilibrium after 144 days of heat injection, after which the heat transfer to the rock is controlled by rock heat conductivity.

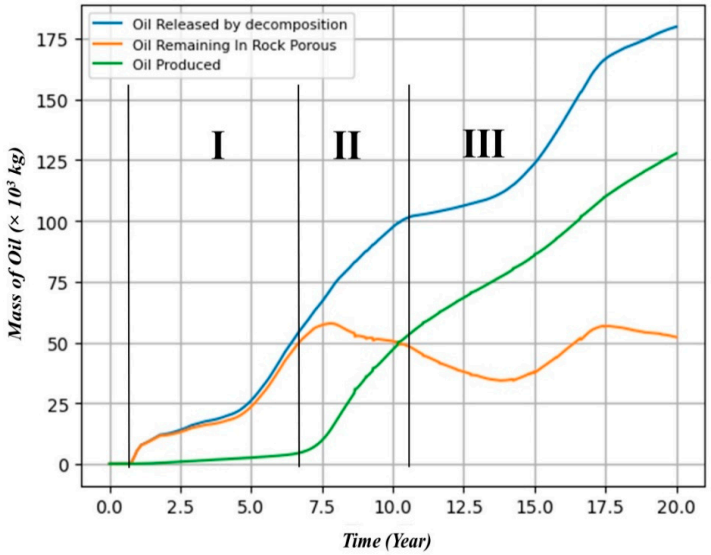

Figure 10. Oil behavior in the reservoir during the in situ conversion process.

In the first phase, oil production increases slowly while the oil generated by decomposition increases. Figure 10 illustrates that the released oil becomes trapped within the porous spaces of the rock. This indicates a limited number of flow channels for the oil in the matrix to reach the producer wellbore. Figure 11a,b demonstrate an increase in oil saturation around the injector wells, corresponding to the oil generated by the decomposition caused by a rise in rock temperature (Figures 12a,b and 13a,b). The slight increase in production can be attributed to the decrease in the viscosity of the oil in place. The space–time evolution of the oil viscosity, as depicted in Figure 14, reveals a rapid decrease in viscosity around the heaters, which extend through the reservoir.

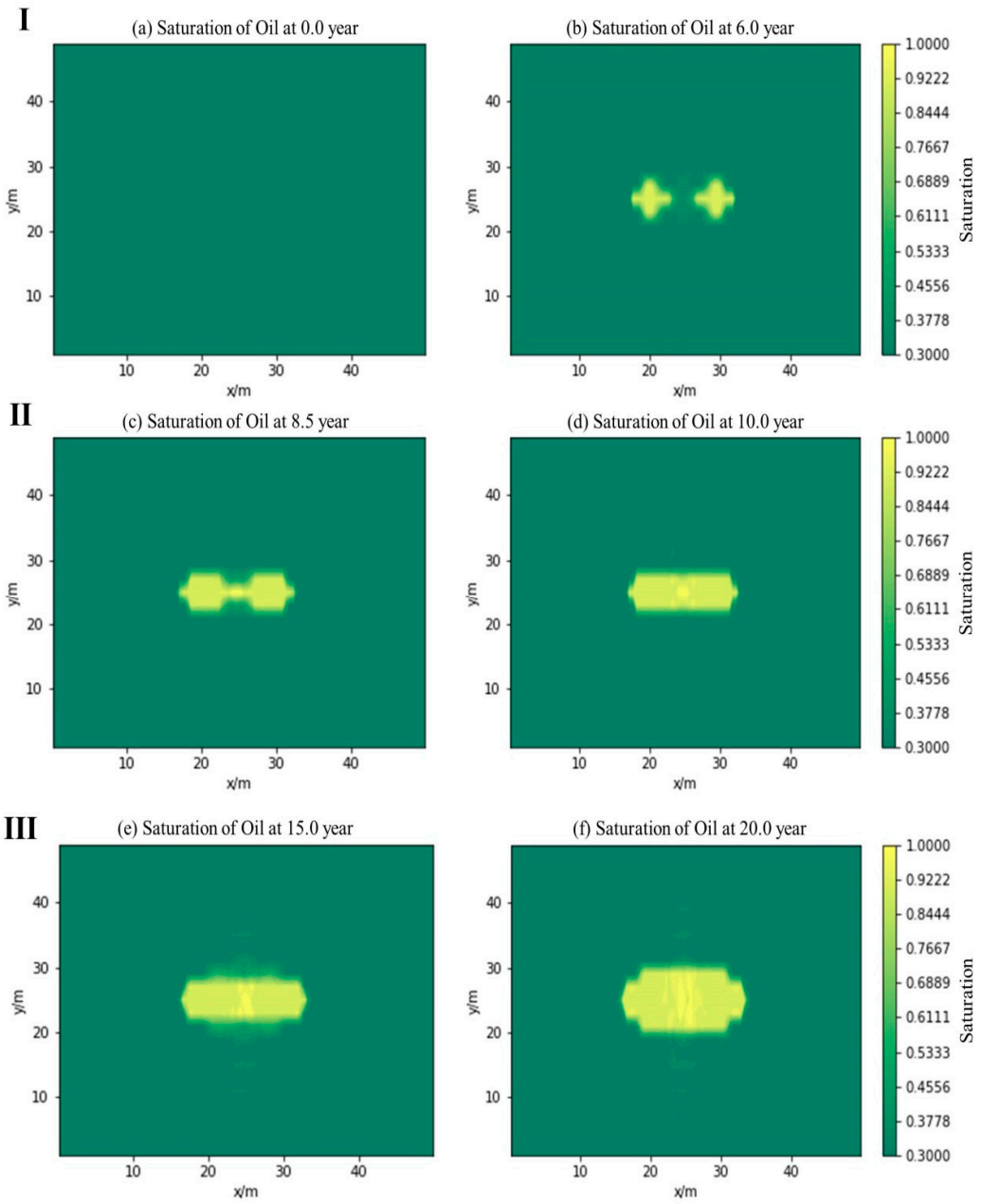

Figure 11. Spatial-time evolution of the oil saturation during the heat injection (**I**–**III**).

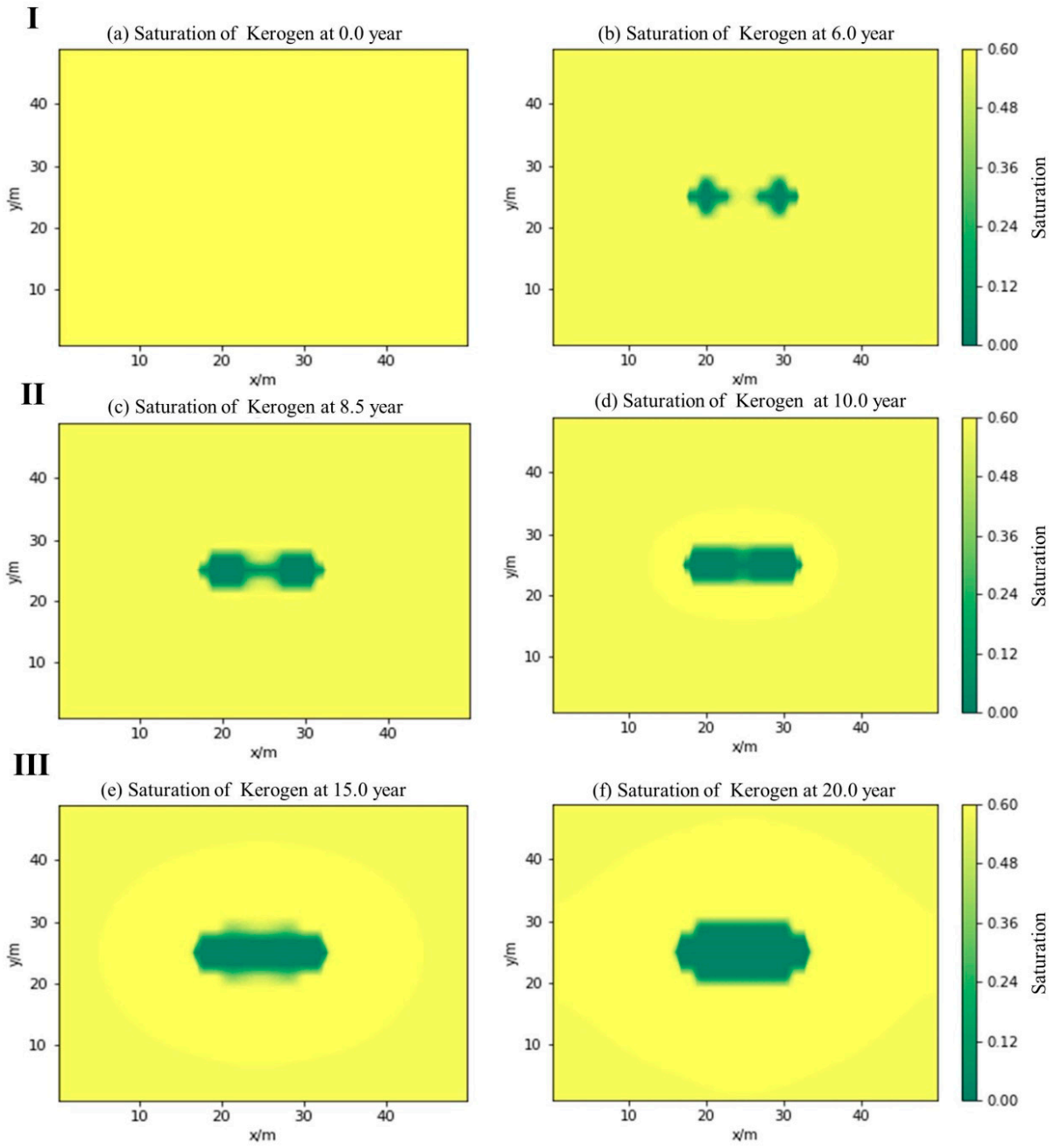

Figure 12. Spatial-time evolution of the kerogen saturation during the heat injection (**I**–**III**).

In the second phase, oil production experiences a sudden increase as the temperature rises in the vicinity of the producer well (Figure 13c,d). This is caused by the kerogen decomposing around the producer, creating free space for the flow of generated oil (Figures 11c,d and 12c,d). As a result, the generated oil continues to increase, while the oil content within the rock starts to decrease.

In the final phase, the generation of liquid oil exhibits a gentle increase between 10 and 14 years of treatment, followed by rapid acceleration. This can be attributed to the low conductivity of the rock, which declines temperature increases in the reservoir (Figure 13e,f). Therefore, the temperature changes affect less of the areas containing organic matter. This phenomenon is evident in the space–time evolution of oil and kerogen saturation (Figures 11e,f and 12e,f). The evolution of the saturated area shows a slow increase after 10 years of treatment. Nonetheless, crude oil production remains to increase

due to the enhanced oil mobility within the porous volume, enabling the efficient drainage of crude oil toward the production well.

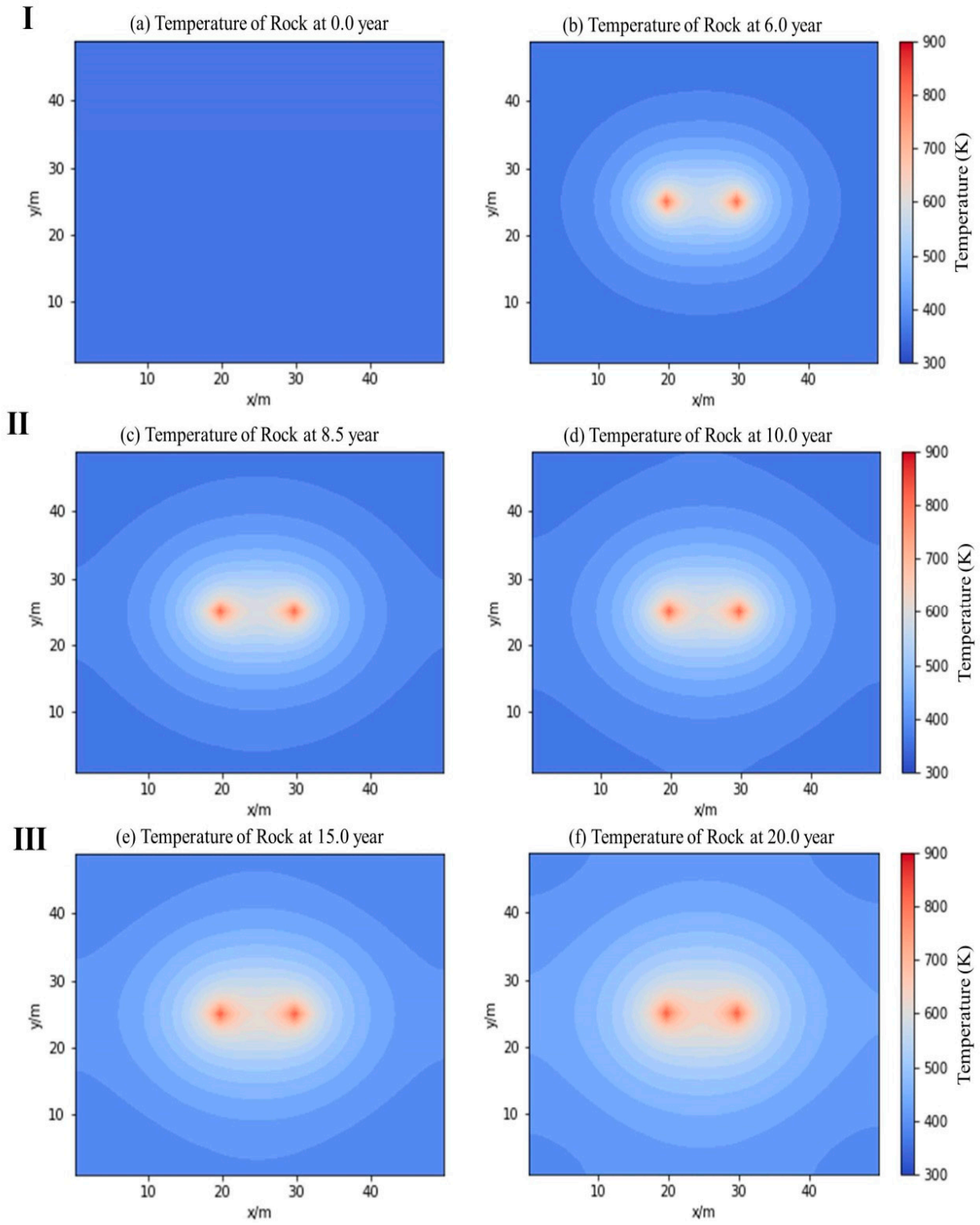

Figure 13. Spatial-time evolution of the rock temperature during the heat injection (**I–III**).

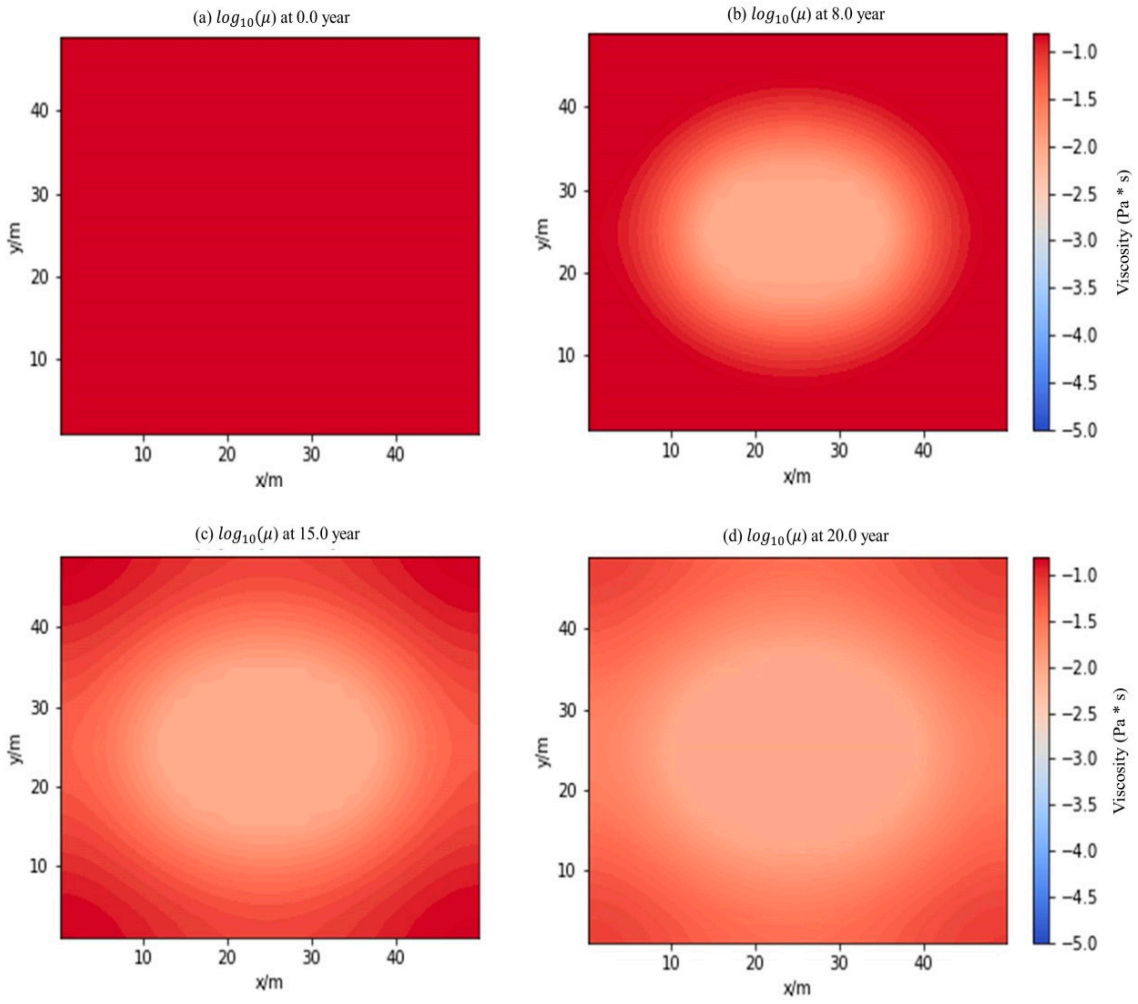

Figure 14. Spatial-time evolution of the oil viscosity during the heat injection.

3.5. Heater Position Effects

The positioning of the heaters plays a crucial role in the in situ treatment. This section conducts several simulations with varying spacing between the heaters and the production well to evaluate the configuration of the wells in the treatment and to analyze the role of well spacing in a shale matrix. The results indicate that oil production increases when the spacing between the producing well and the heaters decreases (Figure 15a). As the temperature near the producer well rises, it can trigger the decomposition of the kerogen, creating free space for the flow of generated oil.

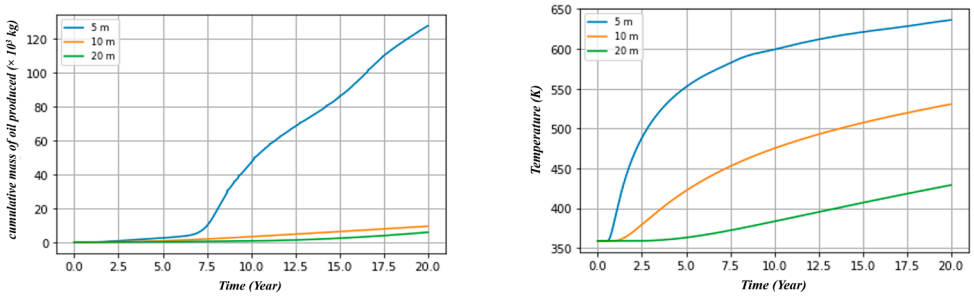

Figure 15. Effects of the spacing between heaters and well producers (**a**) on the accumulation of mass oil produced, and (**b**) on the temperature of the oil produced.

Figure 15b indicates that shorter injection distances lead to increased oil temperatures. Therefore, the closer the heat sources are, the faster that the injection's effect on production becomes noticeable. For instance, at distances of 20 m, the temperature of the fluid around the producer well increases by around 50 K. However, this temperature is not sufficient for improving fluid properties and initiating kerogen decomposition. Figure 16 shows the evolution of the temperature and oil saturation at different heater distances. The temperature surrounding the producer well exceeds 700 K at close range, while it only reaches 500 K at greater distances. This indicates that the thermal in situ conversion technique requires considerable heat sources to increase oil production. Thus, the closer these sources are, the more effective the in situ conversion technique becomes. Additionally, the effects of injection will be observed faster once the in situ heating process has started.

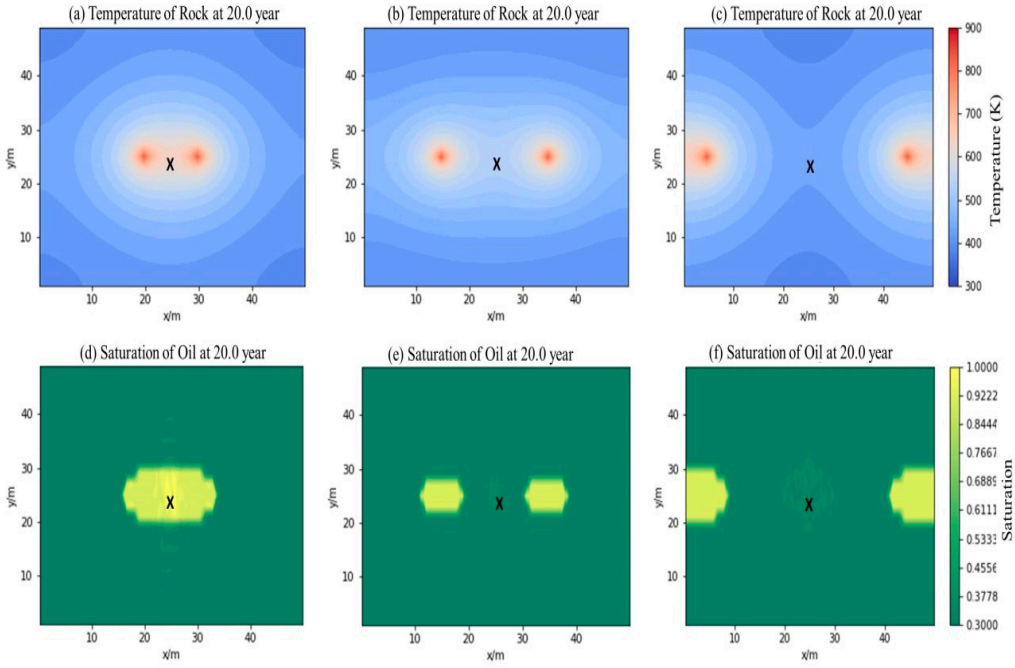

Figure 16. The temperature of rock and the saturation of oil evolution at different heater spacings; (**a**,**d**) temperature distribution at 5 m spacing; (**b**,**e**) temperature distribution at 10 m spacing; and (**c**,**f**) temperature distribution at 20 m spacing. The x indicates the position of the producing well.

3.6. Effects on the Thermal Conductivity Properties

The thermal conductivity properties have significant effects on the in situ conversion process as conductivity heat transfer is the primary factor controlling heat flow. The thermal conductivity of the rock and the heat-transfer coefficient are the key thermal properties involved in the process. To evaluate their impact on oil production and kerogen decomposition, a sensitivity analysis was conducted. The benchmark model serves as the basis for the simulation while each property is evaluated. The injection is set at a constant temperature of 900 K.

The rock heat capacity is defined as the amount of heat absorbed by a material per unit change in temperature. Figure 17a demonstrates that a decrease in rock heat capacity leads to an earlier increase in oil production. A lower heat capacity causes the rock to heat up faster, resulting in more rapid temperature changes through the reservoir. On the other hand, Figure 17b shows that a decrease in rock heat capacity leads to more rapid kerogen decomposition in a shorter period of time. However, the rate of kerogen decomposition decreases gradually decreases over time (indicated by dashed lines in Figure 17b) due to the low conductivity of the rock.

The thermal conductivity of the rock plays a critical role in controlling kerogen decomposition during in situ treatment. As depicted in Figure 18a, an increase in heat conductivity

results in higher oil production. However, if the heat conductivity exceeds 10 W/m·K, the increase in oil production becomes negligible due to the effective permeability of the rock and simulation conditions. Figure 18b indicates that, for heat conductivity values greater than 10 W/m·K, kerogen decomposition is complete after 7.5 years of thermal stimulation. Therefore, after 7.5 years, oil drainage is controlled by the rock's permeability rather than heat conductivity. Figure 19 demonstrates the space–time evolution of the oil saturation and rock temperature at 20 years, revealing that complete kerogen decomposition occurs at a heat conductivity of 15 W/m·K.

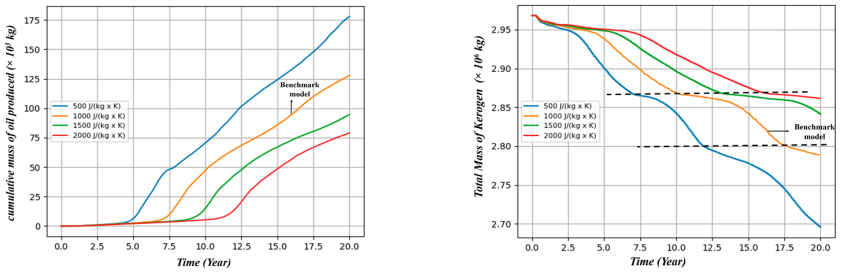

(**a**) (**b**)

Figure 17. Rock heat capacity effects. (**a**) Effects on the mass oil produced, and (**b**) effects on the kerogen decomposition. Dashed lines indicate the effect of the rock heat conductivities that were identified in the benchmark model.

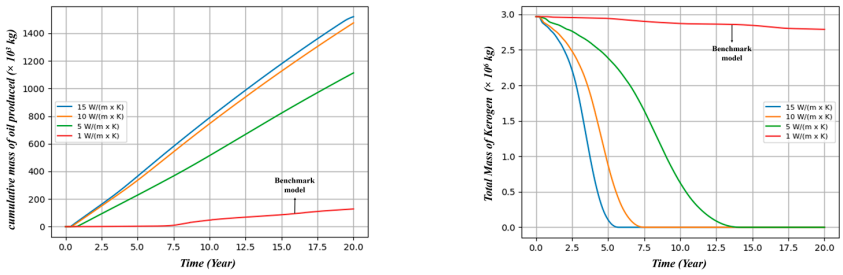

(**a**) (**b**)

Figure 18. Rock heat conductivity. (**a**) Effects on the oil mass production. (**b**) Effects of the rock heat conductivity on kerogen decomposition.

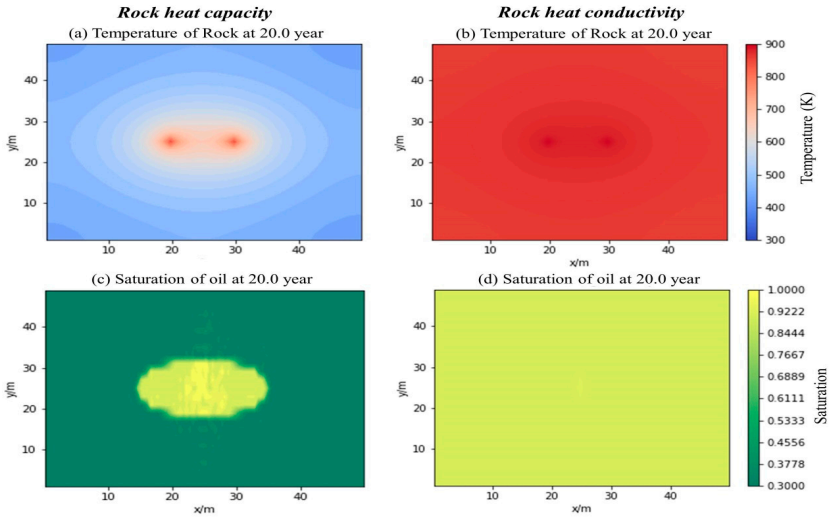

Figure 19. Effects of the limit values of the thermal properties analyzed on the spatial evolution of the oil saturation and temperature of the rock in the reservoir at 20 years of treatment. (**a**,**c**) Correspond to rock heat capacity = 500 J/Kg × K, and (**b**,**d**).

3.7. Effects of the Injection Method

The success of in situ conversion technology is based on its economic viability, which is related to the available surface facilities and the injection capacity required to operate the in situ process. A profitable injection process aims to recover the largest amount of hydrocarbons with the lowest possible injection energy cost. However, the input energy must be sufficient to stimulate a substantial portion of the reservoir. In this study, two boundary conditions are analyzed to assess the role of energy input on recovery efficiency: constant injection temperature and constant heater power (injection energy rate).

Typically, heat injection with electric heaters involves injecting at a constant temperature, where the maximum reservoir temperature reached is equal to the injection temperature. To show the effects of heater temperature, a sensitivity analysis was carried out. Figure 20a illustrates that increasing the injection temperature increases the kerogen decomposition due to the strong dependency of the reaction. However, there are energy losses in the heaters during the treatment process. Figure 20b demonstrates that the energy input (total energy in the heater cells) decreases during the injection due to the heat transfer between the heater and the rock matrix. Conversely, heat injection at constant power (qdt) involves a gradual increase in temperature in the reservoir. Consequently, losses due to heat transfer between the heaters and the rock can be neglected. Figure 21a reveals that increasing the injection power leads to a decrease in kerogen mass, as the reservoir temperature increases over time (Figure 21b), thus resulting in an increased decomposition reaction.

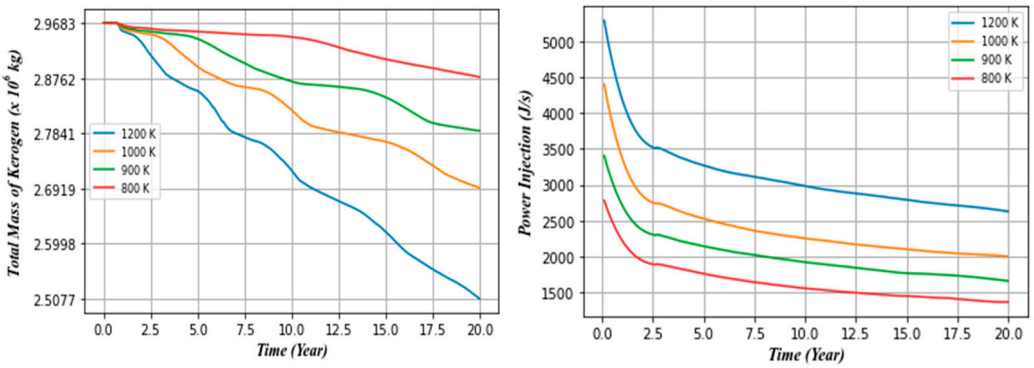

(**a**) (**b**)

Figure 20. Effect of the injection temperature. (**a**) Kerogen decomposition. (**b**) Thermal energy introduced into the formation.

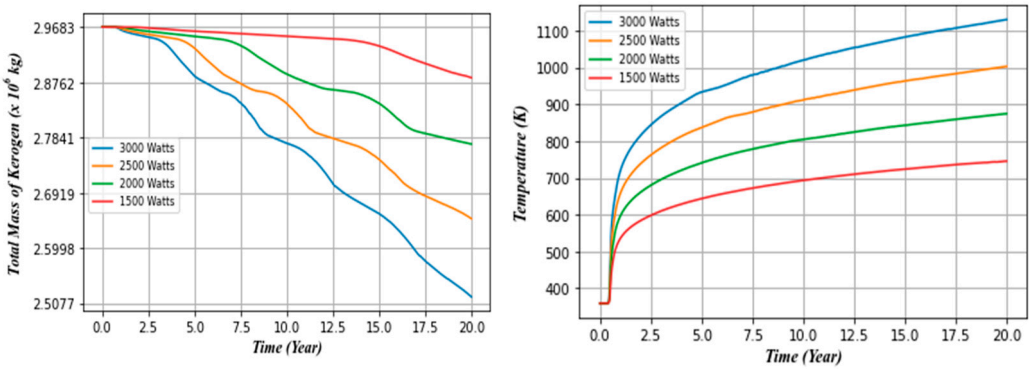

(**a**) (**b**)

Figure 21. Effects of the power constant injection. (**a**) The oil mass accumulated produced. (**b**) Kerogen decomposition.

The effects of kerogen decomposition between a heat injection at constant power and an injection at constant temperature in an oil shale reservoir (Figure 22) were compared.

The figure demonstrates that the decomposition of kerogen increases with constant power injection. This is attributed to the uniform distribution of heat throughout the reservoir that is enabled by a constant power injection. As a result, the temperature of the heaters progressively increases, leading to a more efficient and complete conversion of kerogen. Conversely, injection at a constant temperature causes localized heating, which can result in an incomplete kerogen conversion and the formation of undesired by-products. Therefore, heat injection at a constant power is a more effective method for maximizing the recovery of oil from oil shale reservoirs.

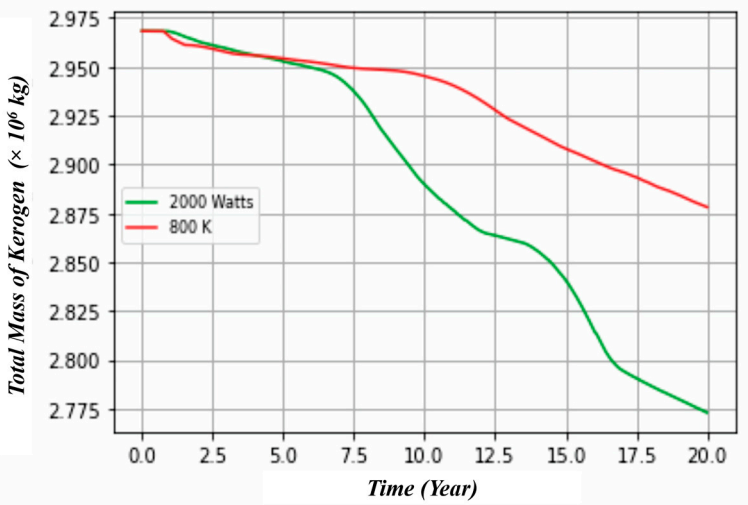

Figure 22. Comparison of the effects of the boundary conditions on kerogen decomposition.

4. Discussion

In the last few years, the in situ conversion process (ICP) has gained attention due to the promising results reported by the Mahogany Demonstration South Project (MDP-S) of the Shell Oil Company in the Green River Formation [38]. This process is a practical method for heating oil shale, which can be applied to all formation depths. However, the sedimentary characteristics of oil shale reservoirs make for difficult oil extraction given that oil shale shows anisotropy in its heat-transfer characteristics [18]. In the electrical injection method, implemented by Shell, the thermal conductivity of the rock controls the temperature evolution. Therefore, changes in thermal conductivity affect the temperature distribution and the efficiency of the method. Then, understanding the thermal process and the effects of thermal parameters is crucial when optimizing the stimulation process and in avoiding unnecessary energy consumption.

The utilization of our self-developed numerical simulation has enabled us to devise an alternative injection approach that is distinct from the Shell ICP method. The horizontal injection scheme affords us a more detailed observation of the temperature evolution within the reservoir, particularly with regard to the effects of injected heat on hydrocarbon production and its correlation with the thermal characteristics of the rock. Furthermore, we conducted an evaluation of heat injection at constant power levels to analyze the role of injected energy in both shale oil production and kerogen decomposition. This exploration has presented a new injection alternative that warrants evaluation in future studies as current injection methods predominantly revolve around heat injection at constant temperatures.

Our analysis reveals that production does not exhibit a direct correlation with the initiation of kerogen decomposition. Instead, there exists a transitional stage where the production rate gradually increases before experiencing a significant surge after a certain period of treatment. Fan et al. [8] and Lee et al. [11] observed an alike pattern, although with a shorter duration between decomposition and the onset of production (approximately 100 days after injection) due to their implementation of multiple energy sources. It is worth noting, however, that their studies do not thoroughly evaluate this particular phenomenon.

In our case, the implementation of a two-injector scheme allows us to explore the temperature distribution profile across the cross-sectional area of the reservoir. This analysis reveals that maximum temperatures are achieved near the injection wells, which gradually diminish as one moves away from these injection points. Consequently, the initial amounts of oil expelled through decomposition predominantly occur in the surrounding regions of the injectors, becoming trapped within the porous spaces of the rock. Once the temperature changes reach the production well, the abrupt production of hydrocarbons initiates. The generated fluids fill the voids left by kerogen, facilitating the fluid flow and accelerating the observation of stimulation effects in the production well. Subsequently, as production begins and the injection of heat continues, the rates of decomposition and production progressively decline. This can be attributed to the stimulated areas moving further away from the heat source, resulting in slower temperature changes within the reservoir. These temperature variations are directly associated with the heat transfer phenomena occurring within the reservoir, which are predominantly governed by the thermal conductivity of the rock. When the rock possesses low conductivity, heat transfer is limited, leading to delayed stimulation effects.

Therefore, our research emphasizes the significance of analyzing heat positions to comprehend the temperature distribution and its impact on oil production during in situ treatment. In 2010, Fan et al. [8] analyzed the effects of the distance between adjacent heaters in the ICP method. However, his study focused on observing the effects of the arrangement in the stimulated areas. In 2023, Huang et al. [12] showed that an efficient triangular arrangement of heaters improves the effects on the production and decomposition of kerogen compared to square or hexagonal patterns. However, their study did not consider the space between the wells. We have examined the effects of the positions of the heaters with respect to the production well. Our analysis revealed that shorter distances between the injector and the producer have a faster effect on the production of hydrocarbons. This benefits the effectiveness of the method since the production of resources is achieved in shorter times.

All the aforementioned analyses highlight the significant role played by the thermal conductivity of rocks in temperature evolution. Generally, fine-grained shale exhibits lower thermal conductivity compared to coarser materials [39]. However, it is essential to consider that lithology, density, humidity, pressure, and other factors have a noticeable influence on the thermal conductivity [16]. Therefore, this study evaluated the effects of this property on shale oil recovery under different values. The results demonstrate that increasing the thermal conductivity of the rock increases the rate of kerogen decomposition [40]. These findings are in line with the behavior of thermal conductivity as described by the diffusivity equation, which governs the rate at which heat is transferred through a material; in addition, in the context of our research, it plays a crucial role in controlling both the rate of thermal stimulation and the rate of kerogen decomposition. However, it should be noted that an increase in thermal conductivity does not guarantee an immediate increase in production if the rock matrix has low permeability. Once complete kerogen decomposition is achieved, the flow of shale oil is predominantly controlled by the rock's permeability. It is noted that this research did not consider changes in the thermal conductivity of the rock with temperature. In reality, the thermal conductivity of the rock can change because of the heating process, which can affect the rate of kerogen decomposition [41].

Considering the challenges associated with injecting heat at a constant temperature for achieving effective temperature evolution in the reservoir, we proposed a new approach that involves evaluating heat injection, and it is based on constant power. Our investigation concluded that injecting heat at a constant power leads to a greater decomposition of kerogen compared to injecting heat at a constant temperature. With constant power injection, the amount of heat supplied to the reservoir remains constant regardless of the temperature; whereas, with constant temperature injection, less energy is required when the temperature in the reservoir increases. However, it is essential to note that while constant power injection may require more energy, it also results in a more efficient conversion

of kerogen to oil, which can ultimately lead to a higher overall recovery of oil from the reservoir. These analyses have a direct correlation with the profitability of the project and the available energy capacity, but this study is beyond the scope of this research.

Regardless, our research presents a new injection approach and highlights the advantages of horizontal injection and constant energy levels, it is important to consider alternative viewpoints and the potential limitations of our proposed method. The practicality and scalability of our horizontal injection scheme on a larger scale may need to be further evaluated, and factors such as cost, infrastructure requirements, and operational complexities should be considered. In addition, it is crucial to acknowledge that our study focuses on a specific reservoir and that the applicability of our approach to other oil shale formations may vary. Furthermore, our findings are based on numerical simulations, which inherently involve certain assumptions and simplifications. In spite of our self-developed simulation model demonstrating the capability to simulate in situ conversion processes, the real-world conditions can be more complex and may introduce additional variables that were not fully captured in our model. Therefore, the generalizability of our results to all oil shale reservoirs should be approached with caution, and further validation through field experiments would be necessary.

5. Conclusions

The self-simulator developed successfully models the chemical decomposition of kerogen, coupled with seepage and non-isothermal temperature models. Additionally, the verification of the numerical model through thermal and chemical experiments indicates the reliability of the developed simulator for the in situ conversion process.

Overall, this research provides valuable insights into the importance of the in situ thermal treatment technique and its potential for shale oil recovery. The results show that the effectiveness of the in situ treatment depends on the optimal distribution and intensity of the heat sources. Insufficient distribution of heat sources can lead to an inadequate thermal stimulation of the kerogen, resulting in suboptimal oil recovery. Therefore, a proper management of the heat injection and distribution is essential for achieving optimal temperature evolution, and for maximizing the rate of kerogen decomposition and oil recovery.

The results of the sensitivity analysis highlight the importance of thermal conductivity in controlling the rate of kerogen decomposition during in situ treatment. However, it is important to consider the broader context of oil production, including the permeability of the rock and the efficiency of fluid flow.

Finally, the analysis of the injection methods indicates that constant power injection is more efficient due to the kerogen decomposition increases. Nonetheless, this method may require more energy compared to constant temperature injection, but it is more effective in converting kerogen to oil, which can ultimately result in higher overall oil recovery from the reservoir.

Author Contributions: Conceptualization, methodology, formal analysis, validation, writing—original draft preparation M.J.B.M.; software, resources, writing—review and editing, Z.Z.; supervision, S.L. and X.L.; resources Y.S.; visualization, S.M. All authors have read and agreed to the published version of the manuscript.

Funding: This research was founded by the National Natural Science Foundation of China [Grant No. 42090023]; the Joint Geological Funds of the National Natural Science Foundation of China [No: U2244223]; the Key Deployment Program of Chinese Academy of Sciences [No. ZDRW-ZS-2021-3-1, YJKYYQ20190043, XDA14040401]; the Scientific Research and Technology Development Project of China National Petroleum Corporation [No. 2022DJ5503]; the CAS Key Technology Talent Program; and the Alliance of International Science Organization (ANSO) Scholarship for Young Talents.

Data Availability Statement: The data presented in this study are available on request from corresponding author.

Acknowledgments: The authors would like to thank the Key Laboratory of Shale Gas and Geoengineering of the Institute of Geology and Geophysics of the Chinese Academy of Science, Beijing.

Conflicts of Interest: The authors declare that they have no known competing financial interests or personal relationships that could have appeared to influence the work reported in this paper.

References

1. Boak, J.; Kleinberg, R. Shale gas, tight oil, shale oil and hydraulic fracturing. In *Future Energy: Improved, Sustainable and Clean Options for Our Planet*; Elsevier: Amsterdam, The Netherlands, 2020; pp. 67–95. [CrossRef]
2. Speight, J. *Shale Oil and Gas Production Processes*; Gulf Professional Publishing: Houston, TX, USA, 2019. [CrossRef]
3. U.S. Energy Information Administration. *Technically Recoverable Shale Oil and Shale Gas Resources: An Assessment of 137 Shale Formations in 41 Countries Outside the United States*; U.S. Energy Information Administration: Washington, DC, USA, 2013.
4. Zou, C.; Yang, Z.; Cui, J.; Zhu, R.; Hou, L.; Tao, S.; Yuan, X.; Wu, S.; Lin, S.; Wang, L.; et al. Formation mechanism, geological characteristics and development strategy of nonmarine shale oil in China. *Pet. Explor. Dev.* **2013**, *40*, 15–27. [CrossRef]
5. Ma, Y.; Zhou, S.; Li, J.; Li, Y.; Chen, K.; Zhang, Y.; Fu, D. Exploring petroleum inside source kitchen': Shale oil and gas in Sichuan Basin. *Sci. China Earth Sci.* **2020**, *63*, 934–953. [CrossRef]
6. Ma, Y.; Zhou, S.; Li, J.; Li, Y.; Chen, K.; Zhang, Y.; Fu, D. Pyrolysis characteristics analysis of Chang-7 oill shale using thermal analysis and pyrolysis-gas chromatograph-mass spectrometry. *Energy Explor. Exploit.* **2018**, *36*, 1006–2021. [CrossRef]
7. Zhang, B.; Yu, C.; Cui, J.; Mi, J.; Li, H.; He, F. Kinetic simulation of hydrocarbon generation and its application to in-situ conversion of shale oil. *Pet. Explor. Dev.* **2019**, *46*, 1288–1296. [CrossRef]
8. Fan, Y.; Durlofsky, L.J.; Tchelepi, H.A. Numerical simulation of the in-situ upgrading of oil shale. *SPE J.* **2010**, *15*, 368–381. [CrossRef]
9. Hazra, K.G. Comparison of Heating Methods for in-situ Oil Shale Extraction. Master's Thesis, Texas A&M University, College Station, TX, USA, 2014. [CrossRef]
10. Egboga, N.U.; Mohanty, K.K.; Balhoff, M.T. A feasibility study of thermal stimulation in unconventional shale reservoirs. *J. Pet. Sci. Eng.* **2017**, *154*, 576–588. [CrossRef]
11. Lee, K.; Moridis, G.J.; Ehlig-Economides, C.A. A Comprehensive simulation model of kerogen pyrolysis for the in-situ upgrading of oil shales. *SPE J.* **2016**, *21*, 1612–1630. [CrossRef]
12. Huang, H.; Yu, H.; Xu, W.; Lyu, C.; Micheal, M.; Xu, H.; Liu, H.; Wu, H. A coupled thermo-hydro-mechanical-chemical model for production performance of oil shale reservoirs during in-situ conversion process. *Energy* **2023**, *268*, 126700. [CrossRef]
13. Shi, Y.; Zhang, Y.; Song, X.; Cui, Q.; Lei, Z.; Song, G. Injection energy utilization efficiency and production performance of oil shale in-situ exploitation. *Energy* **2023**, *263*, 125714. [CrossRef]
14. Abdulagatov, I.M.; Abdulagatova, Z.Z.; Grigor'ev, B.A.; Kallaev, S.N.; Omarov, Z.M.; Bakmaev, A.G.; Ramazanova, A.E.; Rabadanov, K.M. Thermal diffusivity, heat capacity, and thermal conductivity of oil reservoir rock at high temperatures. *Int. J. Thermophys.* **2021**, *42*, 1–27. [CrossRef]
15. Waples, D.W.; Waples, J.S. A review and evaluation of specific heat capacities of rock, minerals, and subsurface fluids. Part 1: Minerals and nonporous rock. *Nat. Resour. Res.* **2004**, *13*, 43–54. [CrossRef]
16. Xiong, J.; Lin, H.; Ding, H.; Pei, H.; Rong, C.; Liao, W. Investigation on thermal property parameters characteristics of rocks and its influence factors. *Nat. Gas Ind. B* **2020**, *7*, 298–308. [CrossRef]
17. Labus, M.; Labus, K. Thermal conductivity and diffusivity of fine-grained sedimentary rocks. *J. Therm. Anal. Calorim.* **2018**, *132*, 1669–1676. [CrossRef]
18. Jin, J.; Liu, J.; Jiang, W.; Cheng, W.; Zhang, X. Evolution of the anisotropic thermal conductivity of oil shale with temperature and its relationship with anisotropic pore structure evolution. *Energies* **2022**, *15*, 8021. [CrossRef]
19. Zhang, Z. IGG-Hydrate: Simulation Program for Gas Hydrate Development-Igghydrate. Gitee-Repository. Available online: https://gitee.com/geomech/hydrate?_from=gitee_search (accessed on 5 April 2023).
20. Zhang, Z.; Xu, T.; Li, S.; Li, X.; Josefina, M. Comprehensive effects of heat and flow on the methane hydrate dissociation in porous media. *Energy* **2023**, *265*, 126425. [CrossRef]
21. Pruess, K.; Oldenburg, C.; Moridis, G. *TOUGH2 User's Guide*, version 2.1; LBNL-43134; Lawrence Berkeley National Lab.: Berkeley, CA, USA, 2012.
22. Wellington, S.L.; Berchenko, I.E.; De Rouffignac, E.P. In Situ Thermal Processing of an Oil Shale Formation to Produce a Desired Product. U.S. Patent US6880633B2, 19 April 2005.
23. Pei, S.; Huang, L.; Zhang, L.; Ren, S. Experimental Study on thermal cracking reactions of ultra-heavy oils during air injection assisted in-situ upgrading process. *J. Pet. Sci. Eng.* **2020**, *195*, 107850. [CrossRef]
24. Pei, S.; Wang, Q.; Zhang, P.; Huang, L.; Zhang, L.; Ren, S. Reservoir simulation of air injection assisted in situ upgrading process via subsurface electrical heating based on the horizontal well. *IOP Conf. Ser. Earth Environ. Sci.* **2021**, *631*, 012057. [CrossRef]
25. Vakhin, A.V.; Onishchenko, Y.V.; Chemodanov, A.E.; Sitnov, S.A.; Mukhamatdinov, I.I.; Nazimov, N.A.; Sharifullin, A.V. The composition of aromatic destruction products of Domanic shale kerogen after aquathermolysis. *Pet. Sci. Technol.* **2019**, *37*, 390–395. [CrossRef]

26. Nasyrova, Z.R.; Kayukova, G.P.; Shunina, E.N.; Islamova, G.G.; Batalin, G.A.; Morozova, E.V.; Vakhin, A.V.; Nurgaliev, D.K. Thermal decomposition of kerogen in high-carbon domanic rock of the romashkino oilfield in sub- and supercritical water. *Energy Fuels* **2022**, *36*, 3549–3562. [CrossRef]
27. Burnham, A.K.; Braun, R.L.; Reinolds, J.G.; Sweeney, J.J. Kinetic and Compositional Model of High-Pressure Kerogen Pyrolysis. In *Sedimentary Basin Geochemistry and Fluid/Rock Interactions Workshop*; U.S Department of Energy: Norman, OK, USA, 1991.
28. Lai, D.; Zhang, J.; Tian, Y.; Gao, S.; Xu, G. Mechanism of kerogen pyrolysis in terms of chemical structure transformation. *Fuel* **2017**, *199*, 504–511. [CrossRef]
29. Braun, R.; Burnham, A. *Chemical Reaction Model for Oil and Gas Generation from Type I and Type II Kerogen*; Lawrence Livermore National Lab.: Livermore, CA, USA, 1993. [CrossRef]
30. Onishchenko, Y.V.; Vakhin, A.V.; Gareev, B.I.; Batalin, G.A.; Morozov, V.P.; Eskin, A.A. The material balance of organic matter of Domanic shale formation after thermal treatment. *Pet. Sci. Technol.* **2019**, *37*, 756–762. [CrossRef]
31. Mehrotra, A.K.; Svrcek, W.Y. Viscosity of compressed Athabasca bitumen. *Can. J. Chem. Eng.* **1986**, *64*, 844–847. [CrossRef]
32. Nourozieh, H.; Kariznovi, M.; Abedi, J. Density and viscosity of athabasca bitumen samples at temperatures up to 200 °C and pressures up to 10 MPa. *SPE Reserv. Eval. Eng.* **2015**, *18*, 375–386. [CrossRef]
33. Lindberg, W.R.; Thomas, R.R.; Christensen, R.J. Measurements of specific heat, thermal conductivity and thermal diffusivity of Utah tar sands. *Fuel* **1985**, *64*, 80–85. [CrossRef]
34. Murdock, J.W. *Fundamental Fluid Mechanics for the Practicing Engineer*; Marcel Dekker, Inc.: Philadelphia, PA, USA, 1994; Volume 5. [CrossRef]
35. Yaws, C.L. *Yaws' Handbook of Thermodynamic and Physical Properties of Chemical Compounds*; Knovel: Beaumont, TX, USA, 2003. Available online: www.knovel.com/knovel2/Toc.jsp (accessed on 5 April 2023).
36. IAPWS. *Revised Release on the IAPWS Industrial Formulation 1997 for the Thermodynamic Properties of Water and Steam*; IAPWS: Lucerne, Switzerland, 2007.
37. Tian, S.; Dong, X.; Wang, T.; Zhang, R.; Zhang, P.; Sheng, M.; Cheng, S.; Zhao, H.; Fei, L.; Street, J.; et al. Surface properties of organic kerogen in continental and marine shale. *Langmuir* **2018**, *34*, 13882–13887. [CrossRef] [PubMed]
38. Ryan, R.C.; Fowler, T.D.; Beer, G.L.; Nair, V. Shell's in situ conversion process-from laboratory to field pilots. *ACS Symp. Ser.* **2010**, *1032*, 161–183. [CrossRef]
39. Midttemme, K. Thermal Conductivity of Sedimentary Rocks-Selected Methodological, Mineralogical and Textural Studies. Doctor of Engineering, Norwegian University of Science and Technology (NTNU); 1997. Available online: https://www.osti.gov/etdeweb/servlets/purl/352949 (accessed on 5 April 2023).
40. Xue, L.; Dai, C.; Wang, L.; Chen, X. Analysis of thermal stimulation to enhance shale gas recovery through a novel conceptual model. *Geofluids* **2019**, *2019*, 4084356. [CrossRef]
41. Ma, Y.; He, L.; Li, S.; Teng, J. Heat transfer of oil shale in a small-scale fixed bed. *J. Therm. Anal. Calorim.* **2015**, *124*, 461–469. [CrossRef]

Disclaimer/Publisher's Note: The statements, opinions and data contained in all publications are solely those of the individual author(s) and contributor(s) and not of MDPI and/or the editor(s). MDPI and/or the editor(s) disclaim responsibility for any injury to people or property resulting from any ideas, methods, instructions or products referred to in the content.